Modeling of laser beam deviation and estimation of link outage due to the presence of air bubbles in the underwater wireless optical communication system

MANDEEP SINGH*, MANINDER LAL SINGH, HARDEEP KAUR, PRIYANKA, SEHAJPAL KAUR
Department of Electronics Technology, Guru Nanak Dev University, Amritsar, Punjab, India

The performance of underwater wireless optical communication (UWOC) system is significantly affected by the air bubbles present in the water. Due to the random interaction of different sized air bubbles with the propagating beam, the received signal gets deviated from the weighted centroid and shows random variations. A Gaussian Mixture Model (GMM) is proposed to estimate these variations. Moreover, to check the feasibility of the proposed model Goodness of Fit (GoF) test is performed which provides excellent results. Additionally, the experimental and theoretical outage probabilities are compared which shows close agreement and hence, verifies the precision of the proposed model.

(Received November 26, 2020; accepted February 10, 2022)

Keywords: Underwater wireless optical communication (UWOC), Air bubbles, Beam wander, Outage probability, Aperture area

1. Introduction

The demand for underwater wireless optical communication (UWOC) has increased many folds due to the ongoing expansion of human activities in ocean environments such as underwater exploration, environmental monitoring, scientific data collection, tactical surveillance, and maritime archeology [1]. Fiber-based systems can be used to provide real-time data transmission in underwater applications but it becomes restrictive for most practical cases due to high deployment cost, lack of flexibility, and operational disadvantages. Traditionally acoustic communication is used to transmit data up to 10 km with some limitations: low data transmission rates (Mega bits/sec), very expensive, high transmission loss and low propagation speeds, etc. The electromagnetic (EM) waves in the radio frequency (RF) range are heavily attenuated by seawater and attenuation increases with the increase in the frequency range. Hence, optical communication is becoming a dominant technology to provide higher bandwidth, high throughput, low time latency, and better compatibility with the underwater ecosystem [2-4]. Despite these advantages, the performance of UWOC gets affected by various propagation effects such as absorption, scattering, underwater turbulence, beam wander, dispersion, beam steering, etc. [5-9]. When an optical beam interacts with the water molecules, the photon energy is lost due to absorption. Additionally, the propagation path is altered from the desired direction due to scattering and the receiver is unable to detect the received photons which further degrades the SNR of the system. The underwater turbulence arises due to random fluctuations in the refractive index of the water along the propagation path due to salinity variations, temperature variations, and air bubbles. The air bubbles in water are generally produced due to the release of various gases, breaking surface waves, and by the wake of ship propellers. The reflection and refraction at the water bubble interface induce fluctuations in the received optical signal and the optical beam deviates from the desired path. These effects limit the viable communication range of UWOC up to 100 m [10]. Hence, a comprehensive study on these degrading effects should be required to accurately model the underwater channel to communicate over long distances.

In recent years, rigorous research activities have been carried out to understand the concept of UWOC both theoretically and experimentally. The absorption and scattering are well modeled using Monte Carlo numerical simulation for different water types [8, 11-14]. Also, [15-16] shows a remarkable increase in communication range for optical code division multiple access (OCDMA) based systems using the point-to-point link in UWOC. Further, the sensitivity of the receiver misalignment can be reduced by increasing the divergence angle of the transmitted Gaussian beam [17]. The effect of underwater turbulence on laser beam propagation has been demonstrated in [18-19]. Also, the researchers in [20-22] have proposed a spatial diversity technique using MIMO transmission to mitigate the effect of underwater turbulence. The effect of underwater turbulence due to the salinity gradient is well modeled using Weibull distribution under given channel conditions [23]. Moreover, the temperature-induced turbulence in the UWOC system is characterized by Generalized Gamma distribution. The effect of air bubbles on laser beam propagation is modeled using the mixture of Exponential-Lognormal distribution in both fresh and salty water [24]. This model does not accurately fit all the channel conditions when the size of the air bubbles is varied. Also, the mathematical modeling of Exponential-

Lognormal distribution is very tough to obtain closed-form expressions for BER and outage probability, etc. Further, the statistical distribution of deviation in the weighted centroid of a laser beam is modeled using lognormal distribution and link outage due to beam wander effect in the turbulent FSO link is evaluated experimentally [25]. However, the refractive index variations caused by the inhomogeneities present in the atmosphere are much different from the sea. This makes the lognormal distribution not appropriate for modeling the seawater. Therefore, there is a need for further investigation of a new statistical model to characterize the laser beam deviation in the UWOC system. In real sea conditions, when an optical signal propagates it encounters many interruptions arising from turbulence, suspended particles, or air bubbles which result in fluctuations in the received optical signal. Depending upon the diameter, number, and distribution of the interruptions present in the sea, the centroid of the beam deviates from its instantaneous position, causing off-sight reception of the beam. This effect leads to a high outage probability due to poor reception of the signal at the receiver. Hence, the link available in the presence of different interruptions becomes a critical performance parameter.

Therefore, this paper experimentally evaluates the performance of the UWOC system considering the turbulent water channel. Different sized air bubbles populations are produced in the water tank to create turbulence in the water. Along with turbulence the beam attenuation coefficient of seawater is also numerically estimated. The air bubble's induced turbulence causes random deviations in the weighted centroid of the laser beam. These random deviations are characterized using GMM. The GoF tests are performed to evaluate the fitness behavior between experimental and modeled curves. Furthermore, the link outage probability is also estimated for all the considered cases and it is compared with the theoretical modeled probabilities which show close agreement with each other and hence, verify the precision of the proposed model. Thus, the proposed GMM serves as a more tractable model when it comes to evaluating the system performance metrics such as link outage probabilities and other parameters. Moreover, Oubei *et. al* showed that moving water has no significant effect on the performance of underwater links [26]. Therefore, the present research is carried out in static underwater channel conditions.

The remainder of this paper is organized as follows: Section 2 describes the basics of a UWOC channel to estimate the total attenuation for different water types. Sections 3 and 4 present the experimental setup and methodology adopted to estimate the beam wandering effect and outage probability calculations. In section 5, the GoF test is presented which is used to check the feasibility of the proposed model. Results and discussions are presented in section 6 along with the proposed model. Finally, the concluding remarks are presented in section 7.

2. Basics of UWOC system

The ocean environment is very harsh and complicated. When an optical beam propagates through seawater, the optical properties of seawater are strongly affected which leads to absorption, scattering, and turbulence phenomena. Due to the interaction of the optical beam with the water molecules and suspended particles in seawater, the photons lose their energy which is called absorption phenomenon and is characterized as absorption coefficient a(λ) where λ is the wavelength of the optical beam propagating through the water. It is the linear combination of the absorption properties of pure seawater $a_w(\lambda)$, the concentration of chlorophyll $a_{cl}(\lambda)$ and color dissolved organic matter (CDOM) which is the sum of humic $a_f(\lambda)$ and fluvic acid $a_h(\lambda)$. The absorption coefficient $a(\lambda)$ is given as [8].

$$a(\lambda) = a_w(\lambda) + a_{cl}(\lambda) + a_f(\lambda) + a_h(\lambda) \quad (1)$$

Thus, the total absorption coefficient becomes:

$$a(\lambda) = a_w(\lambda) + a_c^0(\lambda)\left[\frac{C_c}{C_c^0}\right]^{0.0602} + a_h^0 * C_h * exp(-k_h\lambda) + a_f^0 * C_f * exp\left(-k_f\lambda\right) \quad (2)$$

where $a_c^0(\lambda)$ is the specific absorption coefficient of chlorophyll as a function of wavelength, C_c is the total concentration of chlorophyll in (mg/m^3) with respect to $C_c^0 = 1mg/m^3$, a_h^0 is the specific absorption coefficient of humic acid $(18.828\ \mathrm{m^2/mg})$, $C_h = 0.19334 * C_c * \exp(0.12343(C_c/C_c^0))$ is the concentration of humic acids in (mg/m^3), k_h is the constant $(0.01105\mathrm{nm^{-1}})$, λ is the operating wavelength, a_f^0 is the specific absorption coefficient of fulvic acid $(35.959\mathrm{m^2/mg})$, $C_f = 1.74098 * C_c * \exp(0.12327(C_c/C_c^0))$ is the concentration of fulvic acids in (mg/m^3), $k_f$is the constant $(0.0189\mathrm{nm^{-1}})$.

Also, the propagating photons get to deviate from their original path which results in the temporal and spatial spread of the optical beam which limits the data transmission rate. This effect is termed as a scattering phenomenon and can be represented as scattering coefficient b(λ). The total scattering is the sum of the scattering coefficient of pure water $b_w(\lambda)$, scattering from small particles $b_s^0(\lambda)$ and large particles $b_l^0(\lambda)$ as a function of wavelength. [8].

$$b(\lambda) = b_w(\lambda) + b_s^0(\lambda) * C_S + b_l^0(\lambda) * C_l \quad (3)$$

where $b_w(\lambda) = 0.005826/(m) * (400/\lambda)^{4.322}$ is the pure water scattering coefficient, $C_s = 0.01739(g/mg) * C_c * \exp(0.11631(C_c/C_c^0))$ and $C_l = 0.76284(g/mg) * C_c * \exp(0.03092(C_c/C_c^0))$ are the total concentration of small and large particles in (g/m^3) respectively. The spectral dependencies for scattering coefficients of small

and large particulate matter are $b_s^0(\lambda) = 1.151302(m^2/g) * (400/\lambda)^{1.7}$ and $b_l^0(\lambda) = 0.3411(m^2/g) * (400/\lambda)^{0.3}$. Thus, equation (3) becomes:

$$b(\lambda) = (0.005826/(m) * (400/\lambda)^{4.322}) + (1.151302(m^2/g) * (400/\lambda)^{1.7}) * \left(0.01739(g/mg) * C_c * \exp\left(0.11631(C_c/C_c^0)\right)\right) + (0.3411(m^2/g) * (400/\lambda)^{0.3}) * \left(0.76284(g/mg) * C_c * \exp\left(0.03092(C_c/C_c^0)\right)\right) \quad (4)$$

Therefore, the total loss of energy in seawater that is, attenuation coefficient c(λ) which is the sum of absorption and scattering coefficients can be represented as [8].

$$c(\lambda) = a(\lambda) + b(\lambda) \quad (5)$$

The total attenuation depends upon water type and wavelength of operation. For clear water $a(\lambda)$= 0.114 m^{-1}, b(λ) = 0.037 m^{-1} and the total attenuation coefficient is c(λ) = 0.151 m^{-1}. The water has minimum absorbency in 450-550 nm windows. So, the blue/green region of the visible spectrum can be used to transfer data in the underwater channels.

3. Experimental setup

The underwater channel was simulated in a glass chamber of dimensions 156×35×33 cm^3 and was filled with fresh tap water having a refractive index of 1.33 as shown in Fig. 1. The temperature of the water was kept constant to 25^0 Celsius throughout the study. A 5 mW continuous wave 532 nm green laser diode is used as an optical source at the transmitter. A driver circuit was employed to maintain the constant output radiance of a laser diode. An image acquisition device was employed at the receiver side to capture the spot of the laser beam on the screen. The bubble generation was ensured by six hollow copper pipes having small holes of 0.75 mm, 1 mm, 1.2 mm, 1.5 mm, 1.7 mm, and 2 mm respectively. These pipes were further connected to an air blower. The airflow rate was maintained at around 4 L/min throughout the study. This introduced a steady stream of air bubbles along the length of propagation. Fig. 2 shows the intensity profile of the transmitted and received beam along with the interaction of the propagating beam with the air bubbles. The list of parameters used in the experiment is given in Table 1.

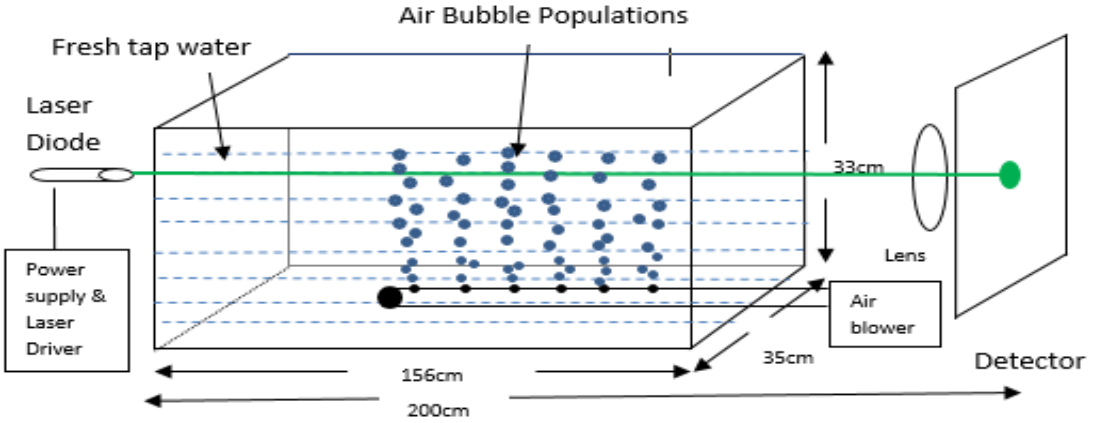

Fig. 1. Experimental setup used in the laboratory

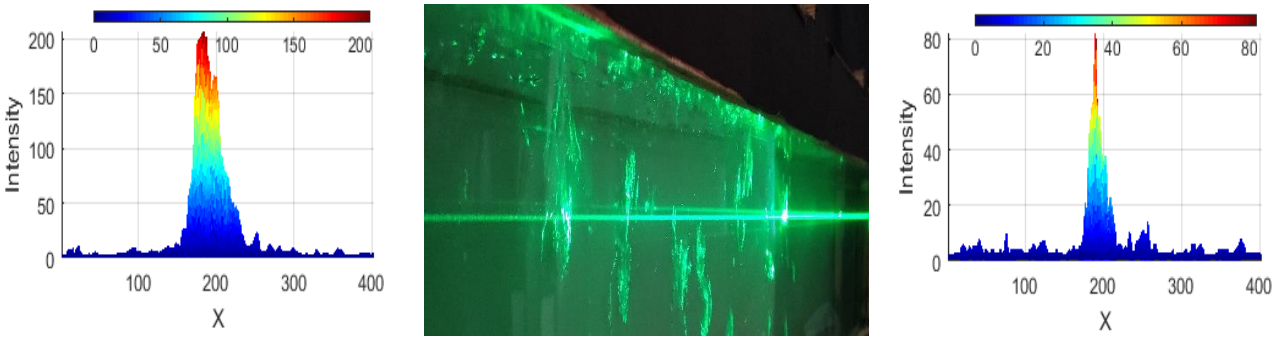

(a) (b) (c)

Fig. 2. (a) Intensity profile of transmitted laser beam (b) Interaction of propagating beam with the air bubbles (c) Intensity profile of received laser beam (color online)

Table 1. Parameters used in the laboratory experiment

S. No.	Parameters	Values
1.	Operating Wavelength	532 nm
2.	Laser power	5 mW
3.	Beam Divergence	0.7 5 mrad
4.	Tx Beam size	0.5 cm
5.	Chamber dimensions	156×35×33 cm^3
6.	Propagation Length	200 cm
7.	Ambient Temperature	20℃
8.	Air blower pressure	0.02 Mpa
9.	Diameter of copper tube	0.5 cm
10.	Length of the copper tube	60 cm
11.	Distance between the holes	7.5 cm
12.	Frame rate for video capturing	60 frames/sec
13.	Pixel Size	0.026 cm
14.	Focal Length	29 mm
15.	Image dimensions	383×337
16.	Aperture Size	f/2.2

4. Methodology

The performance of the UWOC link was evaluated by capturing multiple images of the received spot size in the observation interval. MATLAB was used to process each image of the received spot size. Due to the presence of the air bubbles, the refractive index of the water varies which results in deviation of the beam from the desired path. The beam wandering was estimated by calculating the deviation in the weighted centroid of the laser beam. The centroid is the geometric center of an image where all the pixels of the image are of equal weight whereas pixel intensities of the image are used as weights to calculate the weighted centroid. The weighted centroid is calculated as [25]:

$$\overline{\mathrm{x}} = \frac{\sum_1^{383} \mathrm{I}' x}{\sum_1^{383} \mathrm{I}'} \ , \ \overline{\mathrm{y}} = \frac{\sum_1^{337} \mathrm{I}' y}{\sum_1^{337} \mathrm{I}'} \tag{6}$$

where I' is the intensity value of the pixel of the image, x is the horizontal pixel number, y is the vertical pixel number, $\overline{\mathrm{x}}$ is the horizontal coordinate of the weighted centroid (pixel) and $\overline{\mathrm{y}}$ is the vertical coordinate of the weighted centroid (pixel).

Firstly, in the absence of air bubbles, the average of weighted centroids of all the images was calculated to get a reference weighted centroid. It is incorporated to cancel out the variations other than the variations caused by air bubbles in the water. Further, the displacement of weighted centroid with respect to averaged weighted centroid was calculated in the presence of air bubbles using the following relation [25]:

$$\text{Deviation} = \sqrt{(\mathrm{x}_2 - \mathrm{x}_1)^2 + (\mathrm{y}_2 - \mathrm{y}_1)^2} \tag{7}$$

where $(\mathrm{x}_1, \mathrm{y}_1)$ is the average weighted centroid and $(\mathrm{x}_2 , \mathrm{y}_2)$ is the weighted centroid of the image whose deviation from the weighted centroid has to be calculated.

The performance of the UWOC system is severely affected by suspended organic, inorganic particulate matter and air bubbles present in the water. This causes the optical beam to stray in various directions and the receiver is unable to detect the desired signal. As the generation of air bubbles is a random process, the deviation so caused also exhibits random nature. Thus, the stochastic analysis and the distributions of the above process provide meaningful data that can be further used to model the UWOC system in the presence of air bubbles.

Additionally, in this research paper, the outage probability is estimated to observe the reliability of the UWOC system in the presence of different-sized air bubbles populations. An experimental link outage probability is calculated by comparing the relative position of the weighted centroid with a predetermined threshold. Thus, when the weighted centroid lies outside the threshold aperture area ($\mathrm{A_{th}}$), then link outage occurs and can be calculated by the following relation:

$$\text{Experimental outage probability} = \frac{\sum No.of\ observations\ where\ weighted\ centroid\ lies\ outside\ \mathrm{Ath})}{Total\ No.of\ observations} \tag{8}$$

The theoretical outage probability is calculated from the proposed model and is compared with the theoretical outage for different receiver aperture areas. It is calculated by integrating the area under the distribution curve for $0 < x < \mathrm{A}_{th}$, and then subtracting from unity. Mathematically it can be represented as [25]:

$$P(D \leq x) = \int_0^{\mathrm{A}_{th}} f(x)dx \tag{9}$$

where x is the random variable whose deviation is to be estimated, $f(x)$ is the probability density function of the distribution which gives us the probability that the signal lies within the receiver aperture area. Thus, the predicted outage probability is represented as:

$$\text{Predicted outage probability} = 1 - P(D \leq x) \tag{10}$$

This particular research is focused on estimating link outages due to air bubbles only neglecting other factors.

5. The Goodness of Fit test (GoF)

GoF is used to statistically validate the proposed model by estimating the two well-known metrics such as R-square (R^2) and root mean square error (RMSE). These two metrics prove that how closely our proposed model fits the experimental data under given channel conditions.

The results of R^2 test and RMSE along with the estimated parameters of the proposed model for a given channel condition are listed in Table 3.

5.1. R^2-Test

It is used to test the distribution fitness and it is calculated from the sum of square errors and sum of squares of the distances of the measured point from its mean. It can be expressed as [24]:

$$R^2 = 1 - \frac{SS_{err}}{SS_{tot}} = 1 - \frac{\sum_{i=1}^{N}(P_{m,i} - P_{p,i})^2}{\sum_{i=1}^{N}(P_{m,i} - \bar{P})^2} \quad (11)$$

where N is the total number of measured samples, $P_{m,i}$, $P_{p,i}$ are the experimental and theoretical probabilities for a given received optical power and $\bar{P} = \sum_{i=1}^{N} \frac{IP_{m,i}}{N}$. As the value of $R^2 \to 1$ the proposed model is considered to better fit the experimental data.

5.2. RMSE Test

This test is used to determine how well the considered distribution predicts the experimental data. It can be expressed as [24]:

$$RMSE = \sqrt{\sum_{i=1}^{N} \frac{[I_e(i) - I_p(i)]^2}{N}} \quad (12)$$

where N is the number of measured samples, $I_e(i)$, $I_p(i)$ are the experimental and theoretical predicted values. The lower value of MSE i.e (MSE→0) indicates a better fit and subsequently a better model.

6. Results and discussions

In this section, the performance of underwater wireless optical communication in the presence of air bubbles has been estimated thoroughly. The different air bubble populations are ensured by varying the diameters of the holes in the copper tubes. The air bubbles so generated are of different cross-sectional areas (diameters) and their occurrence is also random in nature. The bubble photographic images are collected using a high-quality camera (resolution 96 dpi) having a frame rate of 60 frames/sec that can directly capture interactions among the air bubbles. A total of 7200 frames are collected and further, these frames are processed in MATLAB to estimate the average bubble area and bubble count for each hole diameter. Fig. 3 shows the distribution of bubble area for different hole diameters.

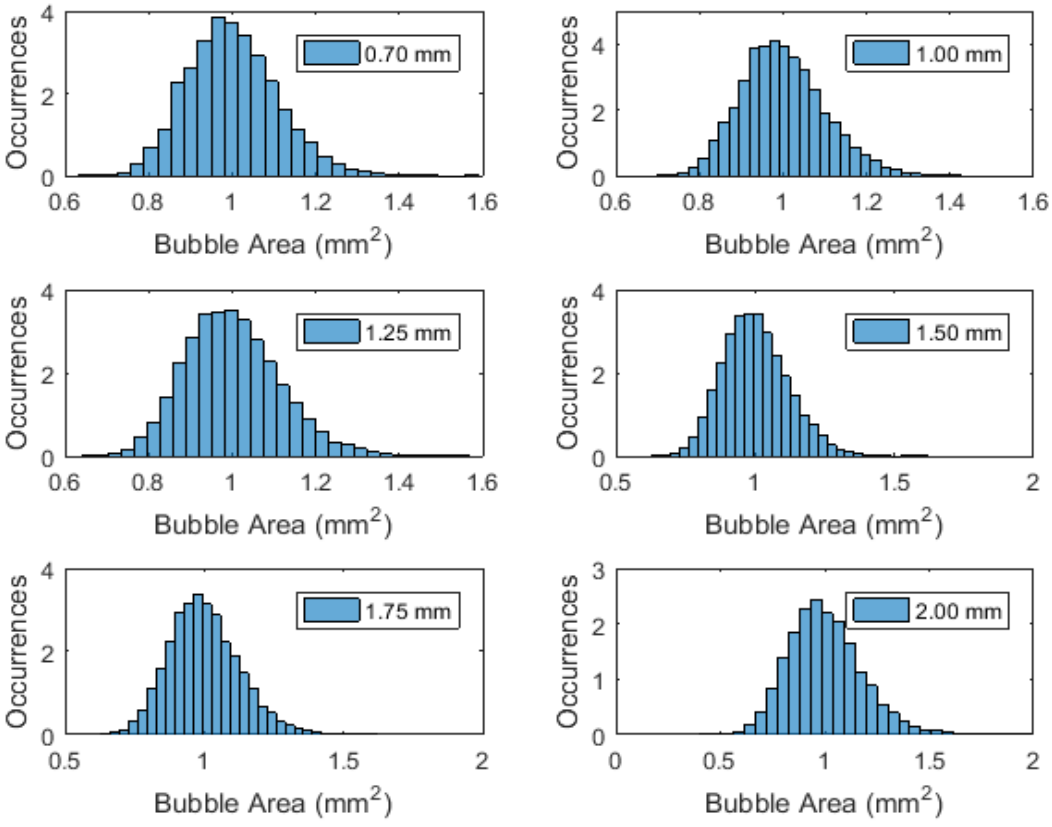

Fig. 3. Histograms of bubble populations for different hole diameters (a) 0.75 mm (b) 1.0 mm (c) 1.2 mm (d) 1.5 mm (e) 1.7 mm (f) 2.0 mm

Table 2. Bubble areas and their density for different hole diameters

Diameter of Hole	Bubbles count (max)	Average Bubble Cross-Sectional Area (mm^2)
0.70 mm	412	1.6078
1.00 mm	470	1.5861
1.25 mm	371	1.6147
1.50 mm	361	1.7915
1.75 mm	328	1.7835
2.00 mm	171	2.3208

The deviation of weighted centroid in the presence of air bubbles is random in nature and the maximum deviation occurred when the air bubbles completely blocked the received optical signal. Thus, the receiver was unable to detect the desired optical signal and leading to high outage probability. The distribution of the deviation in the weighted centroid along with the proposed GMM model is depicted in Fig. 4.

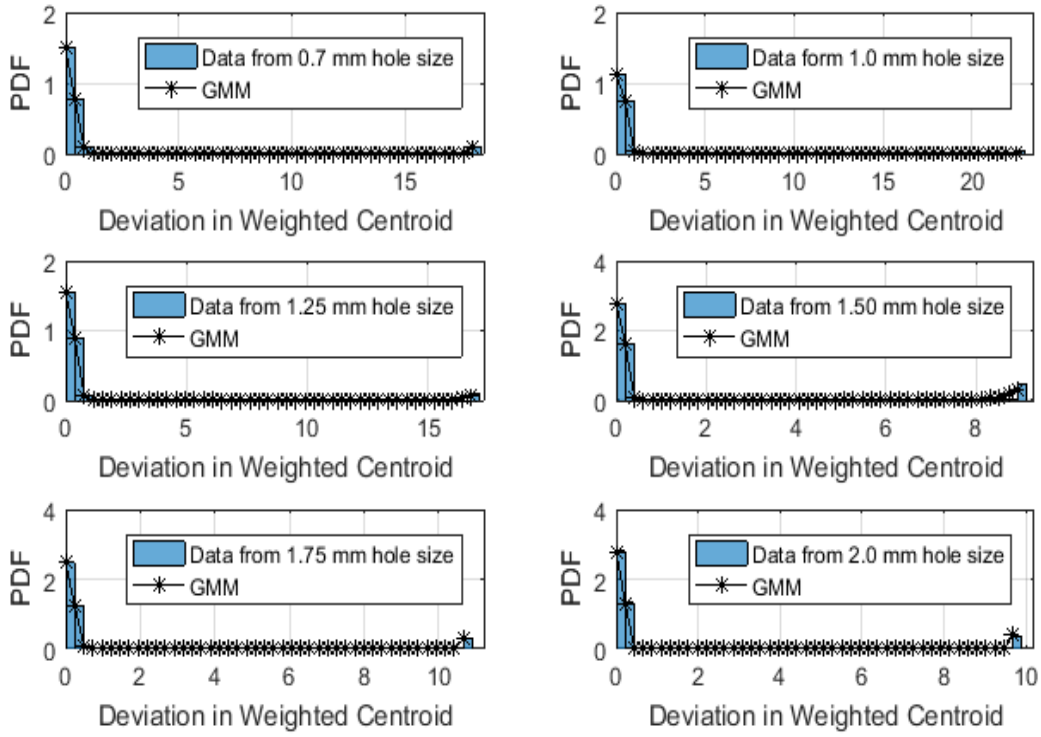

Fig. 4. Distribution of deviation in weighted centroid from the reference weighted centroid with different distributions PDF for different hole diameters (a) 0.75 mm (b) 1.0 mm (c) 1.2 mm (d) 1.5 mm (e) 1.7 mm (f) 2.0 mm

From Fig. 4 it is visible that the deviation in the weighted centroid is well modeled using the Gaussian mixture model (GMM) for all the considered channel conditions. As the diameter of the hole is increased from 0.7 mm to 2.0 mm, bins start rising from the righthand side, and deviation increases. This is due to the fact that with the increase in hole diameter, the average size of the air bubble increases, and bubble count decreases which further decreases the interaction of air bubbles with the propagating beam. The distribution of the proposed GMM model can be expressed as:

$$f(D) = a_1\, exp\left\{-\left(\frac{D-b_1}{c_1}\right)^2\right\} + a_2\, exp\left\{-\left(\frac{D-b_2}{c_2}\right)^2\right\} + a_3\, exp\left\{-\left(\frac{D-b_3}{c_3}\right)^2\right\} \quad (13)$$

where a_1, a_2, a_3 are the amplitudes, b_1, b_2, b_3 are the location parameters, c_1, c_2, c_3 are the scale parameters of the GMM and D is the deviation in the weighted centroid of a laser beam which is estimated from the experiment. The equation (13) represents the weighted sum of three Gaussian functions having mean b_1, b_2 & b_3, variance $c_1/\sqrt{2}$, $c_2/\sqrt{2}$ & $c_3/\sqrt{2}$ and weights assigned are $W_1 = a_1\sqrt{c_1\pi}$, $W_2 = a_2\sqrt{c_2\pi}$ and $W_3 = a_3\sqrt{c_3\pi}$ respectively. The sum of weights i.e. $W_1 + W_2 + W_3 = 1$ is unity. Thus, equation (13) can be represented in general form as:

$$f(D) = \sum_{i=1}^{3} W_i G_i(D; \mu_i, \sigma_i) \quad (14)$$

where G_i is the i[th] normal Gaussian function with mean μ_i, standard deviation σ_i and $\sum_{i=1}^{3} W_i = 1$. The 2[nd] moment of D can be represented as:

$$E[D^2] = \int (D-\mu)^2 f(D) dD = \sum_{i=1}^{3} W_i[{\sigma_i}^2 + (\mu_i - \mu)^2] \quad (15)$$

where E is the expected value of 2nd moment i.e. variance and μ is mean and can be expressed as:

$$\mu = \int D.f(D)dD = \sum_{i=1}^{3} W_i \mu_i \quad (16)$$

The SI_{The} can be obtained from the proposed model as follows:

$$SI_{The} = \frac{\sum_{i=1}^{3} W_i[\sigma_i{}^2+(\mu_i-\mu)^2]}{(\sum_{i=1}^{3} W_i\mu_i)^2} - 1 \quad (17)$$

For the given GMM model, its parameters can be estimated by maximum likelihood estimation using MATLAB. Also, to check the feasibility of the GMM, a GoF test is performed. The parameters of the proposed GMM are evaluated based upon the experimental results, for all the hole sizes are shown in Table 3. In columns 2-10 of Table 3 scale parameters and shape parameters are presented which gives information about distribution shape. Moreover, it is clearly observed that the values of R^2 are very high i.e. close to unity and RMSE close to zero which shows the accuracy of the proposed model. Thus, to model underwater laser beam deviation in the presence of air bubbles, GMM is the most suitable probability distribution that provides the most precise fit with the experimental data collected under all the hole diameters and serves as a most submissive model that provides a lot of analytical facilities to derive easy to use expressions for several performance metrics of UWOC system. The performance parameter, i.e. experimental and modeled outage probability for all the hole sizes is depicted in Fig. 5.

Table 3. Parameters of GMM and GoF test for different channel conditions

Hole Size (mm)	a_1	b_1	c_1	a_2	b_2	c_2	a_3	b_3	c_3	R^2	RMSE
0.70	1.505	0.03069	0.4623	2.44E+12	31.45	2.417	-3.03E-05	10.74	3.528	0.9999	0.0023
1.00	1.281	0.1628	0.4651	0.000902	1.989	0.7946	2.26E+12	126.8	18.37	0.9993	0.0057
1.25	1.629	0.08449	0.3834	4.67E+12	53.13	6.454	4.46E-06	3.511	1.079	0.9991	0.0087
1.50	2.969	0.0488	0.1964	3.34E+13	34.45	4.485	-0.1764	-10.02	5.425	0.9928	0.0446
1.75	2.536	0.03794	0.2424	0.00E+00	-2.862	0.4316	2.29E+13	13.97	0.587	0.9999	0.0028
2.00	2.996	0.04973	0.1875	2.56E+13	12.91	0.573	0.005577	-7.942	7.311	0.9999	0.0018

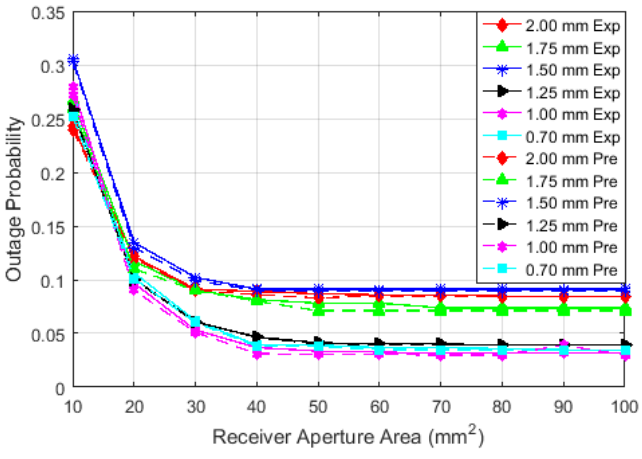

Fig. 5. Comparison of outage probability for different air bubble populations (Exp-experimental outage, Pre- predicted outage) (color online)

Due to the random interaction of air bubbles with the propagating signal, the photons deviate from the desired path which corresponds to outage probability. It is evident from Fig. 5 that the outage probability declines with an increase in the receiver aperture area. For an aperture area of 10 mm^2, the bubbles generated from 1.5 mm and 1.0 mm hole gives a high outage probability. This is due to the fact that the intermediate cases namely 1.0 mm and 1.5 mm have the least variation in bubble area but the bubble count is maximum than other cases which leads to maximum interaction with the propagating beam. As the receiver aperture area is increased, 1.0 mm hole diameter shows the least outage probability due to the least bubble area, and receiver aperture can collect the received optical signal. The outage probability shows a decline up to 40 mm^2 aperture area and after that it becomes constant. This is due to the reason that the deviation in weighted centroid was limited to 15 $pixels^2$ that corresponds to an approximate area of 40 mm^2 as shown in Fig. 5. Whereas after 40 mm^2, the chances of weighted centroid lying outside this aperture area is very less and outage becomes constant. Also, it is clear from Fig. 5 that the experimental outage and theoretically predicted outage probabilities based on the proposed GMM are in close agreement with each other hence, signifying the precision of the theoretical model.

7. Conclusions

In this research paper, based on experimental data the deviation in the weighted centroid of a laser beam in the presence of different sized air bubbles is characterized by the statistical model i.e., the GMM model. This model perfectly matches the measured data, collected under

various channel conditions. The feasibility of this model is estimated by the GoF test by considering a 95 % confidence bound which provides excellent results. It is observed that when most of the air bubbles interact with the propagating beam, they cause the optical beam to spread in various directions and the receiver is unable to detect the desired optical signal resulting in a large outage probability. Thus, the receiver aperture area plays an important role while designing the UWOC system to avoid large outage probabilities. The optimum receiver aperture area for minimizing the link outage probability is approximately 50 mm^2 and the smaller receiver apertures induce large link outages. Furthermore, the theoretically predicted outage probabilities are compared with the experimental values which show close agreement with each other and hence, signifying the precision of the proposed model. Therefore, while designing practical UWOC links in real sea conditions the optimum receiver aperture plays an important role in the faithful transmission of information in the turbulent seawater. The results obtained from the experimental observations are novel which can be considered as a benchmark to estimate the efficiency of the UWOC system. Hence, there is a good scope of future research work in this direction to theoretically analyze the performance of the UWOC system employing advanced transmission/reception techniques.

Acknowledgments

This study has been financially supported by the Department of Electronics and Information Technology (DeitY), Ministry of Electronics and Information Technology (MeitY), Government of India under Visvesvaraya Ph.D. Scheme for Electronics and IT. (Awardee Number - MEITY-PhD-2383).

References

[1] Z. Zeng, S. Fu, H. Zhang, Y. Dong, IEEE Communications Surveys Tutorials **19**(1), 204 (2017).
[2] C. Shen, Y. Guo, H. M. Oubei, T. K. Ng, G. Liu, K. H. Park, K. T. Ho, M. S. Alouini, B. S. Ooi, Opt. Express **24**, 25502 (2016).
[3] H. H. Lu, C. Y. Li, H. H. Lin, W. S. Tsai, C. A. Chu, B. R. Chen, C. J. Wu, IEEE Photonics Journal **8**(5), 1 (2016).
[4] L. Kumar, V. Sharma, A. Singh, Optical Fiber Technology **39**, 78 (2017).
[5] N. B. Mehta, J. Wu, A. F. Molisch, J. Zhang, IEEE Transactions on Wireless Communications **6**(7), 2690 (2007).
[6] S. A. Thorpe, "An Introduction to Ocean Turbulence", Cambridge University Press (2007).
[7] O. Korotkova, N. Farwell, E. Shchepakina, Waves in Random and Complex Media **22**(2), 260 (2012).
[8] W. C. Cox Jr., Simulation, Modeling, and Design of Underwater Optical Communication Systems. Ph. D thesis, North Carolina State University 2012.
[9] X. Li, X. Zhao, P. Zhang, W. Yang, T. Wang, H. Jiang. IET Communications **11**(16), 2476 (2017).
[10] F. Akhoundi, M. V. Jamali, N. B. Hassan, H. Beyranvand, A. Minoofar, J. A. Salehi, IEEE Access **2016**(4), 4254 (2016).
[11] S. Tang, Y. Dong, X. Zhang, IEEE Transactions on Communications **62**(1), 226 (2014).
[12] W. Cox, J. Muth. JOSA A **31**(5), 920 (2014).
[13] H. Zhang, Y. Dong, IEEE Communication Magazine **24**(2), 56 (2016).
[14] B. M. Cochenour, A. Laux, Ocean Sensing and Monitoring VII, **9459,** 94590A (2015).
[15] M. V. Jamali, A. Chizari, J. A. Salehi, IEEE Photonics Technology Letters **29**(5), 462 (2017).
[16] M. V. Jamali, F. Akhoundi, J. A. Salehiet, IEEE Transactions on Wireless Communications **15**(6), 4104 (2016).
[17] Z. Vali, A. Gholami, D. G. Michelson, Z. Ghassemlooy, M. Omoomi, H. Noori, IET Optoelectronics **11**(5), 171 (2017).
[18] M. A. Kashani, M. Uysal, M. Kavehrad, Journal of Lightwave Technology **33**(11), 2303 (2015).
[19] X. Yi, Z. Li, Z. Liu, Applied Optics **54**(6), 1273 (2015).
[20] M. V. Jamali, J. A. Salehi, F. Akhoundi, IEEE Transactions on Communications **65**(3), 1176 (2017).
[21] M. V. Jamali, J. A. Salehi, 4th International Workshop on Optical Wireless Communications (IWOW) IEEE, 26 (2015).
[22] M. V. Jamali, P. Nabavi, J. A. Salehi, IEEE Transactions on Vehicular Technology **67**(9), 8223 (2018).
[23] H. M. Oubei, E. Zedini, R. T. ElAfandy, A. Kammoun, M. Abdallah, T. K. Ng, M. Hamdi, M.-S. Alouini, B. S. Ooi, Opt. Lett. **42**(13), 2455 (2017).
[24] M. V. Jamali, P. Khorramshahi, A. Tashakori, A. Chizari, S. Shahsavari, S. Abdollah Ramezani, M. Fazelian, S. Bahrani, J. A. Salehi, Iran Workshop on Communication and Information Theory (IWCIT'16), Tehran, Iran, 1 (2016).
[25] M. L. Singh, H. S. Gill, M. Singh, S. Kaur, Wireless Personal Communications, **113**(4), 2403 (2020).
[26] H. M. Oubei, R. T. ElAfandy, K. -H. Park, T. K. Ng, M. -S. Alouini, B. S. Ooi, IEEE Photonics Journal **9**(2), 1 (2017).

*Corresponding author: mandeepece.rsh@gndu.ac.in